Azimuthal correlations of high transverse momentum jets at next-to-leading order in the parton branching method

A. Bermudez Martinez[1], L.I. Estevez Banos[1], H. Jung[1], A.M. van Kampen[2], M. Mendizabal[1], S. Taheri Monfared[1], A. Verbytskyi[3], Q. Wang[1,4], and H. Yang[1,4]

[1]Deutsches Elektronen-Synchrotron DESY, Germany
[2]Elementary Particle Physics, University of Antwerp, Belgium
[3]Max-Plank für Physik, Munich, Germany
[4]School of Physics, Peking University

November 25, 2021

Abstract

The azimuthal correlation, $\Delta\phi_{1,2}$, of high transverse momentum jets in pp - collisions at $\sqrt{s} = 13$ TeV is studied by applying PB-TMD distributions to NLO calculations via MCatNLO together with PB-TMD parton shower. A very good description of the cross section as a function of $\Delta\phi_{1,2}$ is observed. In the back-to-back region of $\Delta\phi_{1,2} \to \pi$ a very good agreement is observed with PB-TMD Set 2 distributions while significant differences are obtained with PB-TMD Set 1 distributions, which use the evolution scale as argument in α_{s}, confirming the importance of angular ordering in the parton evolution. The uncertainties of the predictions are dominated by the scale uncertainties of the matrix element, the uncertainties coming from the PB-TMDs and the corresponding PB-TMD shower are very small.

1 Introduction

The description of the cross section of high p_{T} jets in pp collisions is one of the most important tests of predictions in Quantum Chromo Dynamics (QCD), and much progress has been achieved in the description of inclusive jets [1, 1–8] [3, 6, 8–12] by applying next-to-leading [13–16] and next-to-next-to leading order calculations [17–20]. In multijet production, the azimuthal angle $\Delta\phi_{1,2}$ between the two highest p_{T}-jets is an inclusive measurement of additional jet radiation. At lowest order (LO) in α_{s}, where only two jets are produced, the jets are produced back-to-back, $\Delta\phi_{1,2} = \pi$, while a deviation from this back-to-back region indicates the presence of additional jets, and only higher order calculations can describe the observations. The azimuthal correlation between two jets has been measured in $\mathrm{p\bar{p}}$ collisions at a center-of-mass energy of $\sqrt{s} = 1.96$ TeV [21, 22], in pp collisions by the ATLAS Collaboration at $\sqrt{s} = 7$ TeV [23], and by the CMS Collaboration at $\sqrt{s} = 7$, 8, and 13 TeV [24–27]. Calculations at leading and next-to-leading-logarithm have been obtained in [28–30]. The azimuthal correlations of dijets were in general described by calculations at LO supplemented by parton showers or applying higher order matrix element calculations together with parton showers. However, deviations from the measurements of up to 50 % were observed in the medium $\Delta\phi_{1,2}$ region (see e.g. [25, 26]), calling for a more detailed understanding. In the region $\Delta\phi_{1,2} \to \pi$ deviations of up to 10 % are observed [27], significantly large than the experimental uncertainties..

Since initial state parton radiation leads to deviations from the $\Delta\phi_{1,2} = \pi$ region, it is tempting to apply transverse momentum dependent parton distributions (TMD) to describe the $\Delta\phi_{1,2}$ measurements. Especially the region $\Delta\phi_{1,2} \to \pi$ is sensitive to multi-gluon emissions and a resummation is needed. A calculation based on TMD distributions is found in Ref. [29, 30] and further investigated in [31, 32]. However, in this region there are effects, which lead to so-called *factorization - breaking* [33] and it is important to study the importance of those effects by a comparison of calculations assuming factorization with high precision measurements.

The Parton Branching (PB) - method [34, 35] allows to determine transverse momentum dependent (TMD) parton distributions. With these PB-TMD distributions a very good description of Drell-Yan production [36] at the LHC [37] as well as at lower energies [38] is obtained. In Ref. [39] it is shown than $\mathrm{Z+b}$ production is also well described by this method. TMD parton distributions have been used together with off-shell matrix elements at lowest order in Refs. [40, 41] showing a reasonably good description of the measurements.

This article is the result of studies performed during the "virtual Monte Carlo school - PB TMDs with CASCADE3" [42] which was held from 8.-12. November 2021 at DESY, Hamburg, with more than 60 participants and more than 25 participants during the HandsOn exercises. We investigate in detail high p_{T}- dijet production applying the Parton Branching formulation of TMD evolution together with NLO calculations of the hard scattering process in the MADGRAPH5_AMC@NLO [43] framework. We first give a very brief recap of the PB distributions as well as the TMD parton shower Monte Carlo generator CASCADE3 [44]. We then show predictions applying fixed-next-to-leading order calculations and discuss the region where soft gluon resummation becomes important. We show predictions using PB - TMDs together with TMD parton shower. We compare these predictions with one using the PYTHIA8 parton shower mechanism. We finally give conclusions (Sec. 5).

2 PB TMDs and PB method

The PB method as described in Refs. [34, 35] provides a solution of evolution equations for collinear and TMD parton distributions by applying the concept of resolvable and non-resolvable branchings with Sudakov form factors providing the probability to evolve from one scale to another without resolvable branching. The PB is described in more detail in Refs. [35, 45].

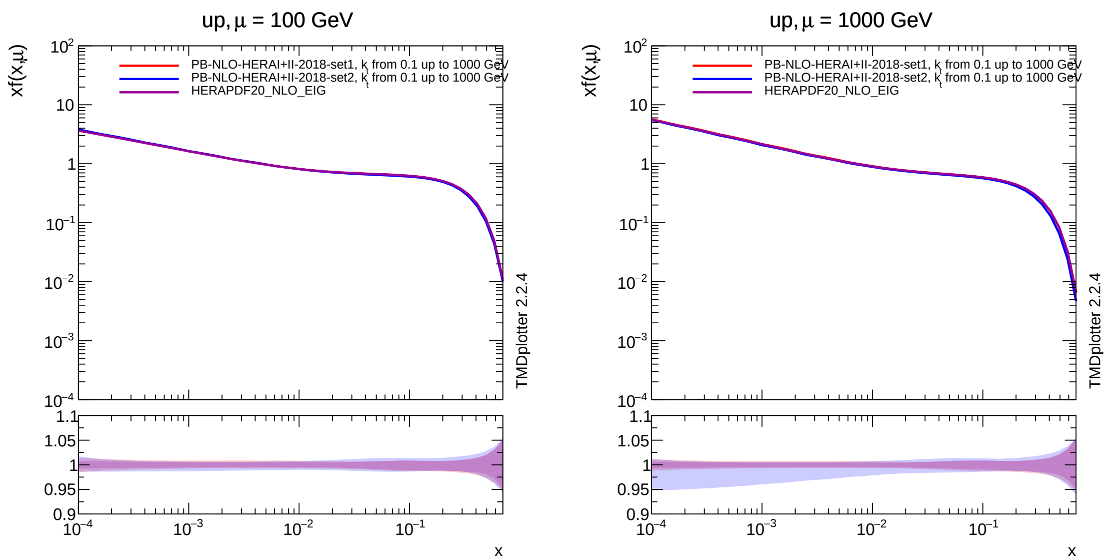

Figure 1: Collinear parton distributions for up quarks (PB-NLO-2018-Set1, PB-NLO-2018-Set 2 and HERAPDF2.0) as a function of x at $\mu = 100$ and 1000 GeV. In the lower panel the uncertainties are shown.

For the numerical calculations we use the next-to-leading order sets, PB-NLO-2018-Set1 and PB-NLO-2018-Set 2, as obtained in Ref. [45] from a fit to inclusive-DIS precision measurements from HERA [46]. Both the collinear and TMD distributions are available in TMDLIB [47], including uncertainty sets. PB-NLO-2018-Set1 corresponds at collinear level to HERAPDF 2.0 NLO [46], and PB-NLO-2018-Set 2 uses transverse momentum (instead of the evolution scale in Set1) for the scale in the running coupling α_s, corresponding to the angular-ordering approach.

In Fig. 1 the Set 1 and Set 2 collinear densities are shown for up-quarks at evolution scales of $\mu = 100$ and 1000 GeV, typical for mulitjet production described below. The collinear densities are also available in a format compatible with LHAPDF [48], and can be used in calculations of physical processes at NLO. In Fig. 2 we show the TMD distributions for up-quarks at $x = 0.01$ and $\mu = 10$ and 100 GeV. The differences between Set 1 and Set 2 are essentially visible in the small k_T-region.

In general it is observed that the uncertainties coming from the TMDs are small, for $k_T >$

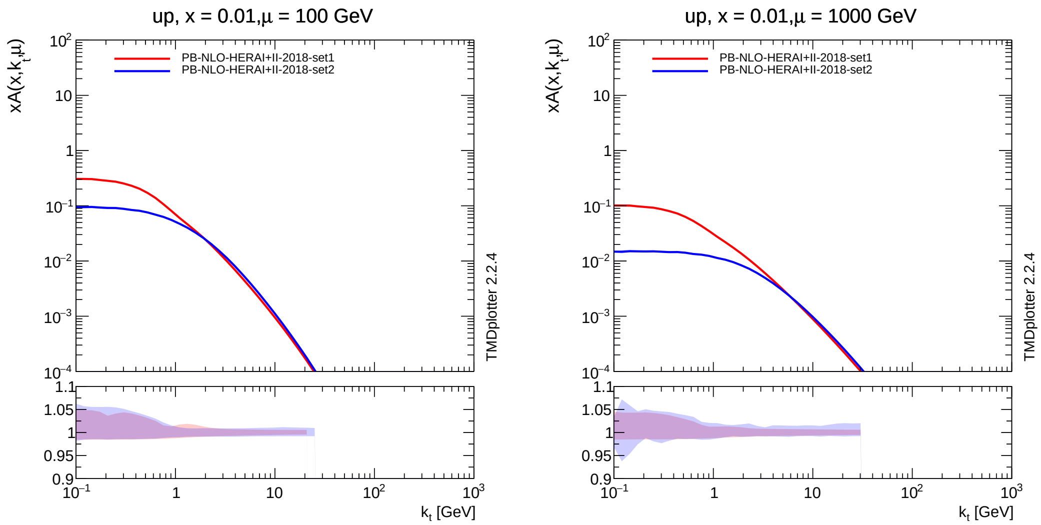

Figure 2: TMD parton distributions for up quarks (PB-NLO-2018-Set1 and PB-NLO-2018-Set 2) as a function of k_{T} at $\mu = 100$ and 1000 GeV and $x = 0.01$. In the lower panels show the full uncertainty of the TMDs, as obtained from the fits [45].

1 GeV they are of the order of 2–3 %.

3 Multijet production at NLO

Multijet production at NLO is performed using the MADGRAPH5_AMC@NLO [43] framework. We used MADGRAPH5_AMC@NLO in two different modes, one is the fixed NLO mode, where only partonic events are produced, without parton shower and hadronization, and the real MC@NLO mode, where subtraction terms are included, and the events need to be supplemented with parton shower in order to provide a physical cross section.

Fixed NLO dijet production is calculated within MADGRAPH5_AMC@NLO framework. Technically, in the fixed NLO mode MADGRAPH5_AMC@NLO produces event files with the partonic configuration in LHE format which can be processed through CASCADE3 combining events and counter events (but without adding TMD or parton shower or hadronization) such, that the they belong to the same event for a proper calculation of statistical uncertainties. Processing through CASCADE3 has the big advantage, that a fixed NLO calculation can be obtained making use of all the analyses coded in Rivet [49].

In the MC@NLO mode, subtraction terms are included which depend on the parton shower used. For the PB-TMDs and the PB-TMD parton shower we use HERWIG6 [50, 51] subtraction terms, as already applied in Z and Drell-Yan analyses (see e.g. [37, 38]), motivated by the angular ordering in the PB evolution. MADGRAPH5_AMC@NLO (version 2.6.4, hereafter labelled MCatNLO) [43] together with the NLO PB parton distributions with

$\alpha_s(M_Z) = 0.118$ is used for NLO calculation of dijet production. The matching scale μ_m which limits the contribution from PB-TMDs, the analogue to that of parton showers, is set to μ_m = SCALUP (included in the LHE file). The factorization and renormalization scale in MCatNLO is set to $\mu_{R,F} = \frac{1}{2}\sum_i \sqrt{m_i^2 + p_{t,i}^2}$ which is also used in the PB- TMD $\mathcal{A}(x, k_T, \mu)$.

As described in detail in Ref. [44] the transverse momentum of the initial state partons is calculated according to the distribution of k_T provided by the PB-TMD $\mathcal{A}(x, k_T, \mu)$ at given x and scale μ. This transverse momentum is used for the initial state partons provided by MCatNLO and their longitudinal momentum is adjusted such that the mass and the rapidity of the dijet-system is conserved, similar to what has been done in the DY case [38]. The initial state TMD parton shower is included in a backward evolution scheme, respecting all parameters and constraints from the PB-TMD. The kinematics of the hard process are not changed by the shower, after the k_T from the TMD is included. The final state parton shower is obtained with the corresponding method implemented in PYTHIA6 [52], using the angular ordering condition.

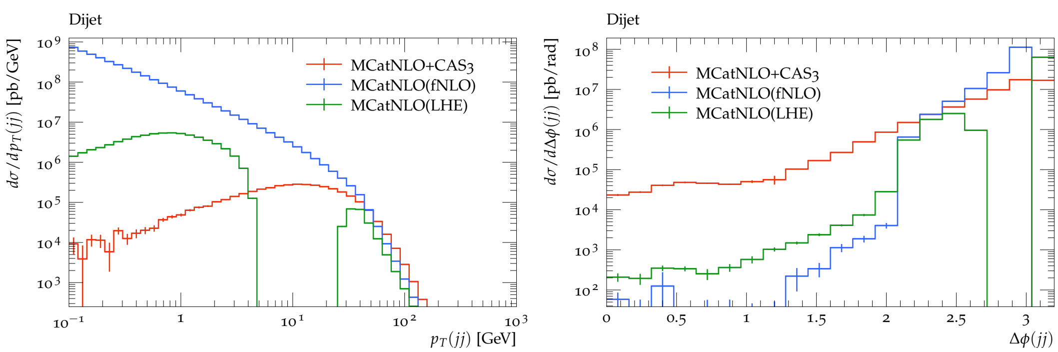

Figure 3: Transverse momentum spectrum of the dijets system (left) and $\Delta\phi_{1,2}$ distribution (right). Shown are predictions form fixed NLO (MCatNLO(fNLO), the (unphysical) LHE level (MCatNLO(LHE)) and after inclusion of PB-TMDs (MCatNLO+CAS3).

In Fig. 3 we show results for the transverse momentum distribution of the dijet system and the azimuthal correlation $\Delta\phi_{1,2}$ between the two leading jets as obtained from the MCatNLO calculation at fixed NLO (blue curve), at the level including subtraction terms (LHE level, green curve) and after inclusion of PB-TMDs (red curve). One can clearly observe the rising cross section of the fixed NLO calculation towards small $p_{T,jj}$ (or at large $\Delta\phi_{1,2}$), the region in $p_{T,jj}$ and $\Delta\phi_{1,2}$where the subtraction terms are relevant and the smooth prediciton obtained when PB-TMDs and parton showers are included. The jets are defined with the anti-k_T jet-algorithm [53], as implemented in the FASTJET package [54], with a distance parameter of R=0.4 and a transverse momentum $p_T > 200$ GeV. The usage of jets (instead of partons) is the reason for the tail towards small $\Delta\phi_{1,2}$ in the MCatNLO(LHE) and MCatNLO(fNLO) calculation.

4 Azimuthal correlations in multijet production

We next apply the framework described in the previous section, based on the matching of PB-TMDs with NLO, to the measurement of azimuthal correlations $\Delta\phi_{1,2}$ obtained by CMS at $\sqrt{s} = 13$ TeV [26] and in the back-to-back region ($\Delta\phi_{1,2} \to \pi$) [27]. Only leading jets with a transverse momentum of $p_{\mathrm{T}}^{\max} > 200$ GeV are considered. We show distributions of $\Delta\phi_{1,2}$ for $p_{\mathrm{T}}^{\max} > 200$ GeVas well as for the very high p_{T} region of $p_{\mathrm{T}}^{\max} > 1000$ GeV, where the jets appear very collimated. We apply the collinear and TMD set PB-NLO-2018-Set 2, unless explicitly specified, with running coupling $\alpha_{\mathrm{s}}(m_{\mathrm{Z}}) = 0.118$. In the calculations, the uncertainty coming from the scale choice is estimated by a variation of the factorization and renormalization scales by a factor of 2 up and down in the 7-point scheme (avoiding the extreme cases of variation). In Fig. 4 we show a comparison of the measurement by

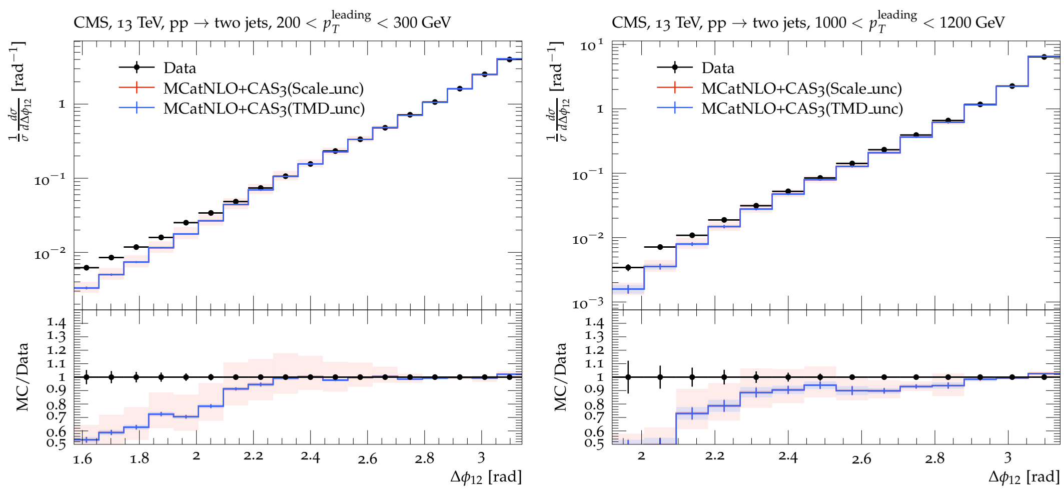

Figure 4: Azimuthal correlation $\Delta\phi_{1,2}$ for $p_{\mathrm{T}}^{\max} > 200$ GeV (left) and $p_{\mathrm{T}}^{\max} > 1000$ GeV (right) as measured by CMS [26] compared with predictions from MCatNLO+CAS3. Shown are the uncertainties coming from the scale variation (as described in the text) as well as the uncertainties coming from the TMD.

CMS [26] for different values of $p_{\mathrm{T}}^{\max}$ with the calculation MCatNLO+CAS3 including PB-TMDs, parton shower and hadronization. The uncertainties from scale variation and TMD determination are shown separately. In Fig. 5 the measured $\Delta\phi_{1,2}$ distribution [27] in the back-to-back region is compared with the prediction MCatNLO+CAS3.

In general the measurements are very well described, especially in the back-to-back region. The scale uncertainty is significantly larger than the TMD uncertainty, especially in the low $p_{\mathrm{T}}^{\max}$ region. A difference between the measurement and the prediction is observed for smaller $\Delta\phi_{1,2}$ which is due to missing higher order corrections in the matrix element calculation. Even at high $p_{\mathrm{T}}^{\max} > 1000$ GeV the predcition is in agreement with the measurements (within uncertainties), only in the highest $\Delta\phi_{1,2}$ bin ($\Delta\phi_{1,2} > 179^o$) a deviation of about 10%

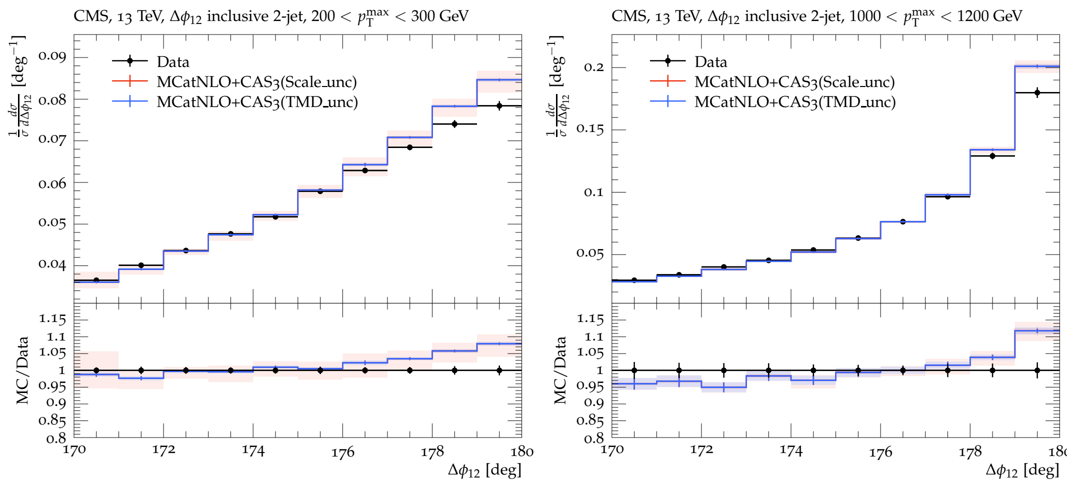

Figure 5: Azimuthal correlation $\Delta\phi_{1,2}$ in the back-to-back region for $p_T^{max} > 200$ GeV (left) and $p_T^{max} > 1000$ GeV (right) as measured by CMS [27] compared with predictions from MCatNLO+CAS3. Shown are the uncertainties coming from the scale variation (as described in the text) as well as the uncertainties coming from the TMD.

is observed.

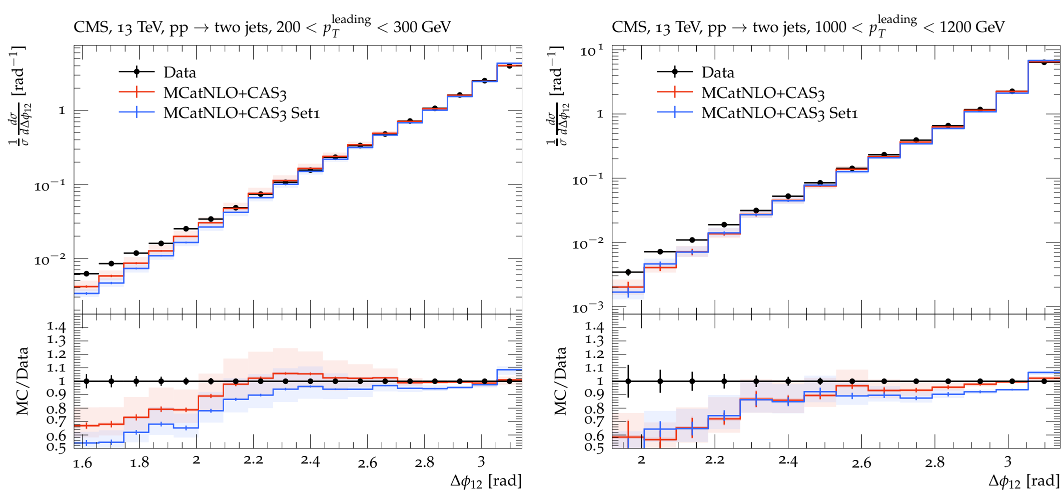

Figure 6: Azimuthal correlation $\Delta\phi_{1,2}$ for $p_T^{max} > 200$ GeV (left) and $p_T^{max} > 1000$ GeV (right) as measured by CMS [26] compared with predictions from MCatNLO+CAS3. Shown are the uncertainties coming from the scale variation (as described in the text) as well as the uncertainties coming from the TMD.

In Fig. 6 and 7 the predictions using PB-NLO-2018-Set 1 are compared with those from

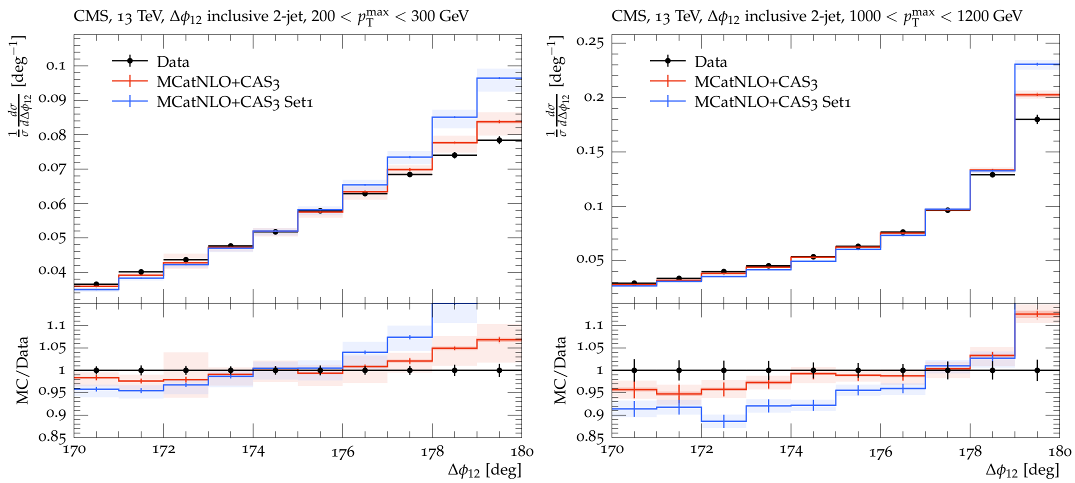

Figure 7: Azimuthal correlation $\Delta\phi_{1,2}$ in the back-to-back region for $p_{\mathrm{T}}^{\max} > 200$ GeV (left) and $p_{\mathrm{T}}^{\max} > 1000$ GeV (right) as measured by CMS [27] compared with predictions from MCatNLO+CAS3. Shown are the uncertainties coming from the scale variation (as described in the text) as well as the uncertainties coming from the TMD.

PB-NLO-2018-Set 2 and the measurements. The difference between Set 1 and Set 2 becomes significant in the back-to-back region, which is sensitive to the low k_{T}-region of the TMD. As already observed in the case of Z-boson production in Ref. [37] Set 2 with the transverse momentum as scale for α_{s}, which is required from angular ordering conditions, allows a much better description of the measurement.

In Fig. 8 predictions obtained with MCatNLO+PYTHIA8 are compared with MCatNLO+CAS3. In the calculation MCatNLO+PYTHIA8, the PYTHIA8 subtraction terms are used and the NNPDF3.0 [55] parton density and tune CUETP8M1 [56] are applied. Shown in Fig. 8 is also the contribution from multiparton intereactions, which is very small for jets with $p_{\mathrm{T}}^{\max} > 200$ GeV. The prediction obtained with MCatNLO+PYTHIA8 is in all $\Delta\phi_{1,2}$ regions different from the measurement and from MCatNLO+CAS3, illustrating the role of the treatment of parton showers.

In conclusion, the predictions of MCatNLO+CAS3 are in reasonable agreement with the measurements in the larger $\Delta\phi_{1,2}$ regions, where the contribution from higher order matrix elements is small. Especially in the back-to-back region ($\Delta\phi_{1,2} \to \pi$) the predictions obtained with PB-TMDs and parton shower are in good agreement with the measurement. The uncertainties of the predictions are dominated by the scale uncertainties of the matrix element calculations, while the PB-TMD and TMD shower uncertainties are very small, as they are directly coming from the uncertainties of the PB-TMDs. No uncertainties, in addition to those from the PB-TMD, come from the PB-TMD parton shower.

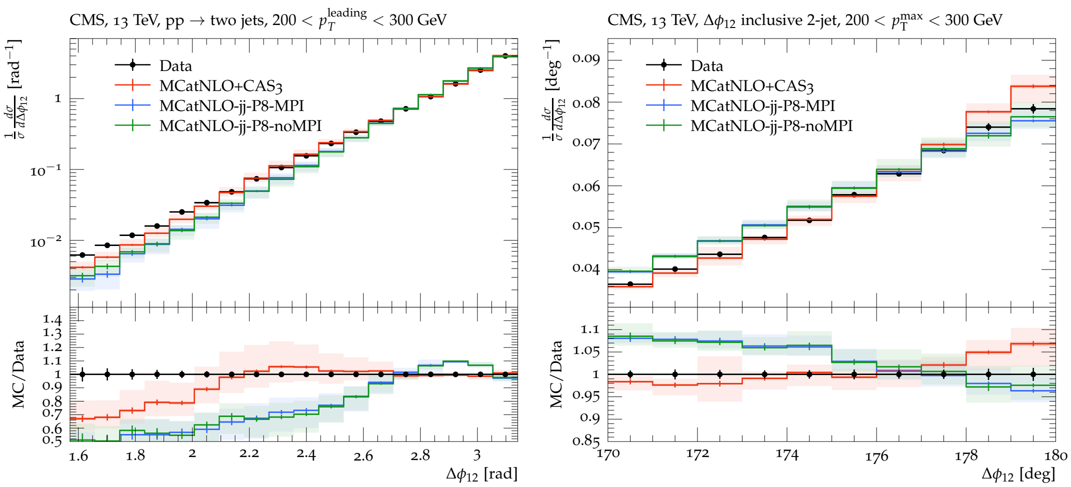

Figure 8: Azimuthal correlation $\Delta\phi_{1,2}$ over a wide range and (left) in the back-to-back region (right) for $p_{\mathrm{T}}^{\max} > 200$ GeV compared with predictions from MCatNLO+PYTHIA8 and MCatNLO+CAS3.

5 Conclusion

We have investigated the azimuthal correlation of high transverse momentum jets in pp - collisions at $\sqrt{s} = 13$ TeV by applying PB-TMD distributions to NLO calculations via MCatNLO. We use the same PB-TMDs and MCatNLO calculations as we have used for Z-production at LHC energies in Ref. [37]. A very good description of the cross section as a function of $\Delta\phi_{1,2}$ is observed. In the back-to-back region of $\Delta\phi_{1,2} \to \pi$ a very good agreement is observed with PB-TMD Set 2 distributions [45] while significant differences are obtained with PB-TMD Set 1 distributions, which use the evolution scale as argument in α_{s}. This observation confirms the importance of angular ordering in the parton evolution.

The uncertainties of the predictions are dominated by the scale uncertainties of the matrix element, uncertainties coming from the PB-TMDs and the corresponding PB-TMD shower are very small. No other uncertainties, in addition to those of the PB-TMD, come from the PB-TMD shower, since it is directly correlated with the PB-TMD density.

Acknowledgments. STM thanks the Humboldt Foundation for the Georg Forster research fellowship and gratefully acknowledges support from IPM.

References

[1] ATLAS Collaboration, "Measurement of the inclusive jet cross section in pp collisions at sqrt(s)=2.76 TeV and comparison to the inclusive jet cross section at sqrt(s)=7 TeV using the ATLAS detector", *Eur. Phys. J. C* **73** (2013), no. 8, 2509, `arXiv:1304.4739`.

[2] CMS Collaboration, “Measurement of the inclusive jet cross section in pp collisions at $\sqrt{s} = 2.76\,\mathrm{TeV}$”, *Eur. Phys. J. C* **76** (2016), no. 5, 265, arXiv:1512.06212.

[3] CMS Collaboration, “Measurements of Differential Jet Cross Sections in Proton-Proton Collisions at $\sqrt{s} = 7$ TeV with the CMS Detector”, *Phys. Rev. D* **87** (2013), no. 11, 112002, arXiv:1212.6660. [Erratum: Phys.Rev.D 87, 119902 (2013)].

[4] CMS Collaboration, “Measurement of the Ratio of Inclusive Jet Cross Sections using the Anti-k_T Algorithm with Radius Parameters R=0.5 and 0.7 in pp Collisions at $\sqrt{s} = 7$ TeV”, *Phys. Rev. D* **90** (2014) 072006, arXiv:1406.0324.

[5] ATLAS Collaboration, “Measurement of the inclusive jet cross-sections in proton-proton collisions at $\sqrt{s} = 8$ TeV with the ATLAS detector”, *JHEP* **09** (2017) 020, arXiv:1706.03192.

[6] CMS Collaboration, “Measurement and QCD analysis of double-differential inclusive jet cross sections in pp collisions at $\sqrt{s} = 8$ TeV and cross section ratios to 2.76 and 7 TeV”, *JHEP* **03** (2017) 156, arXiv:1609.05331.

[7] ATLAS Collaboration, “Measurement of inclusive jet and dijet cross-sections in proton-proton collisions at $\sqrt{s} = 13$ TeV with the ATLAS detector”, *JHEP* **05** (2018) 195, arXiv:1711.02692.

[8] CMS Collaboration, “Measurement of the double-differential inclusive jet cross section in proton–proton collisions at $\sqrt{s} = 13\,\mathrm{TeV}$”, *Eur. Phys. J. C* **76** (2016) 451, arXiv:1605.04436.

[9] CMS Collaboration, “Dependence of inclusive jet production on the anti-k_{T} distance parameter in pp collisions at $\sqrt{s} = 13$ TeV”, arXiv:2005.05159.

[10] ALICE Collaboration, “Measurements of inclusive jet spectra in pp and central Pb-Pb collisions at $\sqrt{s_{\mathrm{NN}}}$ = 5.02 TeV”, arXiv:1909.09718.

[11] ATLAS Collaboration, “Measurement of inclusive jet and dijet production in pp collisions at sqrt(s) = 7 TeV using the ATLAS detector”, *Phys. Rev.* **D86** (2012) 014022, arXiv:1112.6297.

[12] ATLAS Collaboration, “Measurement of Inclusive Jet and Dijet Cross Sections in Proton-Proton Collisions at 7 TeV Centre-of-Mass Energy with the ATLAS Detector”, *Eur. Phys. J. C* **71** (2011) 1512, arXiv:1009.5908.

[13] S. Alioli et al., “Jet pair production in POWHEG”, *JHEP* **04** (2011) 081, arXiv:1012.3380.

[14] Z. Nagy, “Three jet cross-sections in hadron hadron collisions at next-to-leading order”, *Phys. Rev. Lett.* **88** (2002) 122003, arXiv:hep-ph/0110315.

[15] W. T. Giele, E. W. N. Glover, and D. A. Kosower, "The Two-Jet Differential Cross Section at $\mathcal{O}(\alpha_s^3)$ in Hadron Collisions", *Phys. Rev. Lett.* **73** (1994) 2019–2022, arXiv:hep-ph/9403347.

[16] S. D. Ellis, Z. Kunszt, and D. E. Soper, "Two jet production in hadron collisions at order alpha-s**3 in QCD", *Phys. Rev. Lett.* **69** (1992) 1496.

[17] M. Czakon, A. van Hameren, A. Mitov, and R. Poncelet, "Single-jet inclusive rates with exact color at $\mathcal{O}$ (α_s^4)", *JHEP* **10** (2019) 262, arXiv:1907.12911.

[18] A. Gehrmann-De Ridder et al., "Triple Differential Dijet Cross Section at the LHC", *Phys. Rev. Lett.* **123** (2019), no. 10, 102001, arXiv:1905.09047.

[19] J. Currie, E. W. N. Glover, and J. Pires, "Next-to-Next-to Leading Order QCD Predictions for Single Jet Inclusive Production at the LHC", *Phys. Rev. Lett.* **118** (2017), no. 7, 072002, arXiv:1611.01460.

[20] J. Currie et al., "Single Jet Inclusive Production for the Individual Jet p_{T} Scale Choice at the LHC", *Acta Phys. Polon.* **B48** (2017) 955–967, arXiv:1704.00923.

[21] D0 Collaboration, "Measurement of dijet azimuthal decorrelations at central rapidities in $p\bar{p}$ collisions at $\sqrt{s} = 1.96$ TeV", *Phys. Rev. Lett.* **94** (2005) 221801, arXiv:hep-ex/0409040.

[22] D0 Collaboration, "Measurement of the combined rapidity and p_T dependence of dijet azimuthal decorrelations in $p\bar{p}$ collisions at $\sqrt{s} = 1.96$ TeV", *Phys. Lett. B* **721** (2013) 212–219, arXiv:1212.1842.

[23] ATLAS Collaboration Collaboration, "Measurement of dijet azimuthal decorrelations in pp collisions at sqrt(s)=7 TeV", *Phys.Rev.Lett.* **106** (2011) 172002, arXiv:1102.2696.

[24] CMS Collaboration, "Dijet Azimuthal Decorrelations in pp Collisions at sqrt(s) = 7 TeV", *Phys. Rev. Lett.* **106** (2011) 122003, arXiv:1101.5029.

[25] CMS Collaboration, "Measurement of dijet azimuthal decorrelation in pp collisions at $\sqrt{s}$ = 8 TeV", *Submitted to: Eur. Phys. J. C* (2016) arXiv:1602.04384.

[26] CMS Collaboration, "Azimuthal correlations for inclusive 2-jet, 3-jet, and 4-jet events in pp collisions at $\sqrt{s} = 13$ TeV", *Eur. Phys. J.* **C78** (2018) 566, arXiv:1712.05471.

[27] CMS Collaboration, "Azimuthal separation in nearly back-to-back jet topologies in inclusive 2- and 3-jet events in pp collisions at $\sqrt{s} = 13$ TeV", *Eur. Phys. J. C* **79** (2019) 773, arXiv:1902.04374.

[28] A. Banfi, M. Dasgupta, and Y. Delenda, "Azimuthal decorrelations between QCD jets at all orders", *Phys. Lett. B* **665** (2008) 86–91, arXiv:0804.3786.

[29] P. Sun, C. P. Yuan, and F. Yuan, “Soft Gluon Resummations in Dijet Azimuthal Angular Correlations in Hadronic Collisions”, *Phys. Rev. Lett.* **113** (2014), no. 23, 232001, arXiv:1405.1105.

[30] P. Sun, C. P. Yuan, and F. Yuan, “Transverse Momentum Resummation for Dijet Correlation in Hadronic Collisions”, *Phys. Rev.* **D92** (2015), no. 9, 094007, arXiv:1506.06170.

[31] Y. Hatta, B.-W. Xiao, F. Yuan, and J. Zhou, “Azimuthal angular asymmetry of soft gluon radiation in jet production”, *Phys. Rev. D* **104** (2021), no. 5, 054037, arXiv:2106.05307.

[32] Y. Hatta, B.-W. Xiao, F. Yuan, and J. Zhou, “Anisotropy in Dijet Production in Exclusive and Inclusive Processes”, *Phys. Rev. Lett.* **126** (2021), no. 14, 142001, arXiv:2010.10774.

[33] J. Collins and J.-W. Qiu, “k_T factorization is violated in production of high-transverse-momentum particles in hadron-hadron collisions”, *Phys. Rev.* **D75** (2007) 114014, arXiv:0705.2141.

[34] F. Hautmann et al., “Soft-gluon resolution scale in QCD evolution equations”, *Phys. Lett. B* **772** (2017) 446, arXiv:1704.01757.

[35] F. Hautmann et al., “Collinear and TMD quark and gluon densities from Parton Branching solution of QCD evolution equations”, *JHEP* **01** (2018) 070, arXiv:1708.03279.

[36] S. Drell and T.-M. Yan, “Massive Lepton Pair Production in Hadron-Hadron Collisions at High-Energies”, *Phys.Rev.Lett.* **25** (1970) 316–320.

[37] A. Bermudez Martinez et al., “Production of Z-bosons in the parton branching method”, *Phys. Rev. D* **100** (2019) 074027, arXiv:1906.00919.

[38] A. Bermudez Martinez et al., “The transverse momentum spectrum of low mass Drell–Yan production at next-to-leading order in the parton branching method”, *Eur. Phys. J. C* **80** (2020) 598, arXiv:2001.06488.

[39] S. P. Baranov et al., “Discriminating the heavy jet production mechanisms in associated Z + heavy flavor events at the LHC”, arXiv:2111.04521.

[40] F. Hautmann and H. Jung, “Angular correlations in multi-jet final states from kt-dependent parton showers”, *JHEP* **10** (2008) 113, arXiv:0805.1049.

[41] M. Bury et al., “Calculations with off-shell matrix elements, TMD parton densities and TMD parton showers”, *Eur. Phys. J. C* **78** (2018) 137, arXiv:1712.05932.

[42] A. Bermudez Martinez, H. Jung, S. Taheri Monfared, Q. Wang, "Virtual Monte Carlo school - PB TMDs with CASCADE". https://indico.desy.de/event/31877/, 2021.

[43] J. Alwall et al., "The automated computation of tree-level and next-to-leading order differential cross sections, and their matching to parton shower simulations", *JHEP* **1407** (2014) 079, `arXiv:1405.0301`.

[44] S. Baranov et al., "CASCADE3 A Monte Carlo event generator based on TMDs", *Eur. Phys. J. C* **81** (2021) 425, `arXiv:2101.10221`.

[45] A. Bermudez Martinez et al., "Collinear and TMD parton densities from fits to precision DIS measurements in the parton branching method", *Phys. Rev. D* **99** (2019) 074008, `arXiv:1804.11152`.

[46] ZEUS, H1 Collaboration, "Combination of measurements of inclusive deep inelastic $e^{\pm}p$ scattering cross sections and QCD analysis of HERA data", *Eur. Phys. J. C* **75** (2015), no. 12, 580, `arXiv:1506.06042`.

[47] N. A. Abdulov et al., "TMDlib2 and TMDplotter: a platform for 3D hadron structure studies", *Eur. Phys. J. C* **81** (2021) 752, `arXiv:2103.09741`.

[48] A. Buckley et al., "LHAPDF6: parton density access in the LHC precision era", *Eur. Phys. J. C* **75** (2015) 132, `arXiv:1412.7420`.

[49] A. Buckley et al., "Rivet user manual", *Comput. Phys. Commun.* **184** (2013) 2803–2819, `arXiv:1003.0694`.

[50] G. Corcella et al., "HERWIG 6.5 release note", `arXiv:hep-ph/0210213`.

[51] G. Marchesini et al., "HERWIG: A Monte Carlo event generator for simulating hadron emission reactions with interfering gluons. Version 5.1 - April 1991", *Comput. Phys. Commun.* **67** (1992) 465–508.

[52] T. Sjöstrand, S. Mrenna, and P. Skands, "PYTHIA 6.4 physics and manual", *JHEP* **05** (2006) 026, `arXiv:hep-ph/0603175`.

[53] M. Cacciari, G. P. Salam, and G. Soyez, "The anti-k_t jet clustering algorithm", *JHEP* **04** (2008) 063, `arXiv:0802.1189`.

[54] M. Cacciari, G. P. Salam, and G. Soyez, "FastJet User Manual", *Eur. Phys. J. C* **72** (2012) 1896, `arXiv:1111.6097`.

[55] NNPDF Collaboration, "Parton distributions for the LHC Run II", *JHEP* **04** (2015) 040, `arXiv:1410.8849`.

[56] CMS Collaboration, "Event generator tunes obtained from underlying event and multiparton scattering measurements", *Eur. Phys. J. C* **76** (2016) 155, arXiv:1512.00815.